Environ. Sci. Technol. **2010,** *44,* 8308–8313

Evidence for Bioavailability of Au Nanoparticles from Soil and Biodistribution within Earthworms (*Eisenia fetida*)

JASON M. UNRINE,*,† SIMONA E. HUNYADI,§ OLGA V. TSYUSKO,† WILLIAM RAO,† W. AARON SHOULTS-WILSON,† AND PAUL M. BERTSCH†,‡

Department of Plant and Soil Science, Tracy Farmer Institute for Sustainability and the Environment, University of Kentucky, Lexington, Kentucky 40546, United States, and Savannah River National Laboratory, United States Department of Energy, Aiken, South Carolina 29803, United States

Received June 2, 2010. Revised manuscript received September 14, 2010. Accepted September 16, 2010.

Because Au nanoparticles (NPs) are resistant to oxidative dissolution and are easily detected, they have been used as stable probes for the behavior of nanomaterials within biological systems. Previous studies provide somewhat limited evidence for bioavailability of Au NPs in food webs, because the spatial distribution within tissues and the speciation of Au was not determined. In this study, we provide multiple lines of evidence, including orthogonal microspectroscopic techniques, as well as evidence from biological responses, that Au NPs are bioavailable from soil to a model detritivore (*Eisenia fetida*). We also present limited evidence that Au NPs may cause adverse effects on earthworm reproduction. This is perhaps the first study to demonstrate that Au NPs can be taken up by detritivores from soil and distributed among tissues. We found that primary particle size (20 or 55 nm) did not consistently influence accumulated concentrations on a mass concentration basis; however, on a particle number basis the 20 nm particles were more bioavailable. Differences in bioavailability between the treatments may have been explained by aggregation behavior in pore water. The results suggest that nanoparticles present in soil from activities such as biosolids application have the potential to enter terrestrial food webs.

Introduction

The increased application of nanotechnology in the past decade has raised concerns about both human health and safety and environmental impacts resulting from exposure to engineered nanomaterials (*1*−*4*). Recent studies suggest that NPs may be released from products through normal use and then enter wastewater streams (*5*). A significant portion of NPs in wastewater are expected to partition to sewage sludge (*6, 7*). Depending on local practices, varying proportions of sewage sludge are disposed of in landfills, incinerated, or applied to agricultural lands as biosolids. In the United States, parts of Europe and the United Kingdom, as much as 60% of sewage sludge is applied to the land (*8*). Therefore, terrestrial ecosystems are expected to be an ultimate sink for a large portion of NPs (*9*). This raises concerns about potential for ecological effects, entry in to food webs, and ultimately human exposure from consumption of contaminated agricultural products. Therefore, it is of great interest to determine if intact NPs can be taken up by organisms from soil.

Au NPs have been investigated extensively for use as a contrast agent in electron microscopy, optical sensors, catalysts and for therapeutic uses (*10*−*12*). Because Au metal is extremely resistant to oxidation, it is essentially insoluble under ambient conditions (*13*). It can be synthesized in a variety of sizes and shapes, easily conjugated via thiol chemistry making it amenable to surface modification, and it is readily detected using a variety of analytical and imaging techniques. These properties have led to the use of Au as a probe of particle specific uptake in biological systems ranging from cells to food webs (*14, 15*). Relatively few studies have investigated the uptake of Au NPs from environmentally relevant exposure scenarios, such as from dietary, soil, or sediment exposure (*15*). Although Au is resistant to oxidative dissolution, it is possible for excess Au ions to remain in the product when synthesized, stabilized by excess Cl^- ions from $HAuCl_4$ used as a starting material. Therefore, the possibility that Au associated with organisms was taken up as Au ions cannot be discounted without determination of the speciation of Au in the target tissues and exposure media. This may be of particular importance for materials for which the yield is low, such as nanorods (*16*). Furthermore, bulk chemical analysis of whole organisms does not equivocally demonstrate uptake and distribution of the materials in of itself. For example, organisms may only have Au NPs sorbed onto exterior surfaces or in gut contents which have not been cleared (*15*).

The purpose of this study was to investigate the bioavailability of NPs in soil ecosytems, using Au NPs as a stable probe, the earthworm *Eisenia fetida* as a model detritavore, and soil as an exposure medium. Earthworms were exposed to thoroughly characterized 20, and 55 nm Au particles which were synthesized using citrate reduction methods. For comparative purposes and to provide a positive control for ion uptake, we also exposed earthworms to soils containing $HAuCl_4$. We hypothesized that uptake and toxicity of the Au NPs into tissues would decrease with increasing primary particle size. In order to resolve potential uncertainty about speciation of Au and localization of Au NPs within organisms, we used an approach which combined laser ablation inductively coupled plasma mass spectrometry (LA-ICP-MS), synchrotron based X-ray microspectroscopy (μSXRF), and expression of the metallothionein gene (*mtl*) to provide characterization of exposure, uptake and biodistribution of Au. Toxicity end points included expression of several genes related to oxidative stress and macromolecular damage as well as effects on growth, mortality, and reproduction.

Experimental Section

Synthesis and Characterization of Au NPs. Stable aqueous suspensions of Au spheres with well-defined size (20 or 55 nm), and negative surface charge were prepared by citrate-reduction method using 99.99% $HAuCl_4$ and >99% sodium citrate (Sigma-Aldrich, St. Louis, Mo) (*17*). These colloidal Au nanospheres were centrifuged twice and redispersed in 18 MΩ deionized (DI water) to eliminate the residuals from the reaction. Methods used for material characterization (chemical composition, primary particle size distribution,

* Corresponding author e-mail: jason.unrine@uky.edu.
† Department of Plant and Soil Science.
§ United States Department of Energy.
‡ Tracy Farmer Institute for Sustainability and the Environment.

10.1021/es101885w
© 2010 American Chemical Society
Published on Web 09/29/2010

free ion concentration and particle hydrodynamic diameter in suspension) are described in the Supporting Information (SI).

Bioassay. The design of the earthworm reproduction, bioaccumulation and subchronic lethality assays followed published guidelines (*18*). We added 10 fully clitelate, adult *E. fetida* with an average mass of 0.386 g and a SD (standard deviation) of 0.110 g to each of three replicate exposure chambers containing 500 g dry mass of artificial soil medium. The soil medium consisted of 70% quartz sand, 10% peat moss, and 20% kaolin. The pH was adjusted with the addition of a small amount of crushed limestone. The cation exchange capacity was 0.1445 meq g^{-1}. The particle size distribution was 79.12% sand, 6.71% silt, and 14.17% clay. Appropriate quantities of the Au suspensions and DI water were added to the dry soil and mixed by hand for 5 min to result in nominal concentrations of 5, 20, and 50 mg Au kg^{-1} dry mass and a final moisture content of 30% w/w. Because pilot experiments indicated that $HAuCl_4$ was much more bioavailable and toxic than Au NPs, we limited the nominal concentrations to 2.5, 10, and 25 mg Au kg^{-1} dry mass. These concentrations are similar to those expected for other NPs, such as ZnO, Ag, and TiO_2 in biosolids amended soil (*9*). Control soil was spiked with a sodium citrate solution corresponding to the maximum concentration used during particle synthesis. Soil pH as determined in 1 M KCl solution was 7.6 (*18*) and was unaffected by treatment ($p < 0.05$). Soil subsamples were taken at the beginning of the exposure from each exposure chamber. After 28 days of exposure, three earthworms from each exposure chamber were frozen in liquid nitrogen immediately, while the remaining earthworms were allowed to void their gut contents on moistened filter paper for 24 h and stored frozen for total Au analysis or fixed in formalin for sectioning. Production of juveniles was assessed after 56 days (see SI for details). We determined bulk Au concentrations in soil and whole earthworms using microwave digestion (*19*) in *aqua regia* followed by analysis by ICP-MS (*20*) (see SI for details). Hydrodynamic diameter of particles in pore water was determined using asymmetrical field flow fractionation (AF4; Eclipse 3, Wyatt Technologies, Goleta, CA) with ICP-MS as an Au specific detector (see SI for details).

Laser Ablation ICP-MS. Two dimensional elemental plots of glycol methacrylate cross sections (embedding and sectioning described previously (*21*)) were produced using LA-ICP-MS in order to establish the tissue distribution of Au. We produced elemental plots by creating a series of line scans across the sample surface using a 213 nm laser ablation system (CETAC Technologies, LSX 213, Omaha, NE, USA) coupled to an ICP-MS (Agilent 7500cx) set to $m/z = 196$ and an integration time of 0.05 s. The stage motor position timings from the LA instrument were used to correlate ICP-MS data with sample *x*, *y* coordinates. The data were then smoothed and plotted as contour maps using Sigma Plot 8.0 (SPSS, Chicago, IL).

Synchrotron X-ray Microspectroscopy. Au nanoparticles, soils, and glycol methacrylate embedded tissue sections were analyzed using μSXRF as described previously (*21*). All X-ray analyses were conducted at beamline X-26A, National Synchrotron Light Source (NSLS), Brookhaven National Laboratory (Upton, NY; see SI for details). We produced elemental maps of the samples using scanning X-ray fluorescence mode (spot size approx $6 \times 10\ \mu m^2$). Once areas of high Au accumulation were identified, Au L edge micro-X-ray absorbance near-edge spectroscopy (μXANES) was performed in fluorescence mode. The monochromator was calibrated to the absorption edge of an Au foil. We analyzed Au (0) foil and $HAuCl_4$ standards and compared the absorption edge positions to those of the standards. XANES data were processed and analyzed using the Athena as described previously (*21*, *22*).

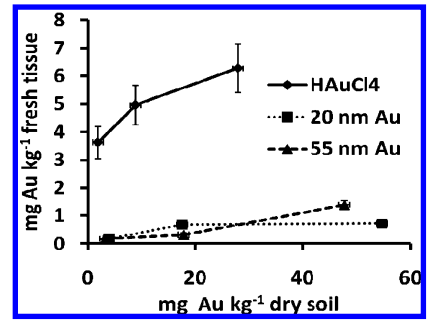

FIGURE 1. Accumulation of Au in earthworms (*Eisenia fetida*) exposed to either $HAuCl_4$, 20 nm Au nanoparticles or 55 nm Au nanoparticles. Error bars indicate standard deviations.

TEM of Tissues. We examined sections of the gut epithelial cells of earthworms from a separate exposure at the highest exposure concentrations for the presence of intracellular particles using transmission electron microscopy (TEM). We used energy dispersive spectroscopy (EDS) for confirmation of elemental content of selected electron-dense features (see SI for a more detailed description).

Quantitative Real-Time Polymerase Chain Reaction (qRT-PCR). We performed qRT-PCR analysis for expression of several genes including: metallothionein (mtl), superoxide dismutase (sod), catalase (cat), heat shock protein 60 (hsp60), heat shock protein 70 (hsp70), and ubiquitin (ubq). β-actin (β-act) was used as a reference gene. The procedures for RNA extraction, purification, reverse transcription, qRT-PCR analysis, quality control, primer sequences and Genbank accession numbers for the target gene sequences have been described previously (*21*). We quantified gene expression for the six target genes using relative expression software tool (REST, ref *23*).

Results and Discussion

Material Characterization. The geometric primary particle diameters as measured by TEM were 20.5 ± 0.7 (mean ± standard deviation) and 54.9 ± 0.7 nm, respectively. The TEM analysis indicated that the particles were spherical and relatively monodisperse (SI Figure S1). The intensity weighted (Z-average) hydrodynamic diameters in deionized water were 33.7 and 70.2 nm, respectively. Au concentrations in the 3 kDa (equivalent pore size is approximately 0.9 nm) filtrates ranged from 1.5×10^{-3} to 1.0×10^{-2} % of the stock suspension total Au concentrations after correction for 60% recovery. This indicated that residual reactants in the suspension were removed during washing and that concentrations of free Au ions were extremely low. This was confirmed by μXANES, since the spectra for the suspensions were nearly identical to the spectra from an Au foil reference standard (SI Figure S2). The pH of the 20 nm stock suspension was 8.06, which was only slightly higher than the soil pH. The 55 nm suspension caused an interference with the pH electrode (perhaps by clogging the junction); however, according to pH indicator paper, the pH value was approximately 8. The electrophoretic mobilities of the samples were −3.14 and −3.20 μM cm V^{-1} s^{-1} corresponding to zeta potentials of −60.0 and −61.4 mV ($F_{ka} = 1.5$) for 20 and 55 nm suspensions, respectively. This confirmed that the two suspensions had similar pH values since the electrophoretic mobilities of the particles were not significantly different.

Exposure Characterization. The actual concentrations achieved in the soil were similar to the nominal concentrations and homogeneity was evidenced by close agreement in Au concentration (Mean RPD = 6%) among subsamples of the soil (Figure 1). The μXANES analysis indicated that

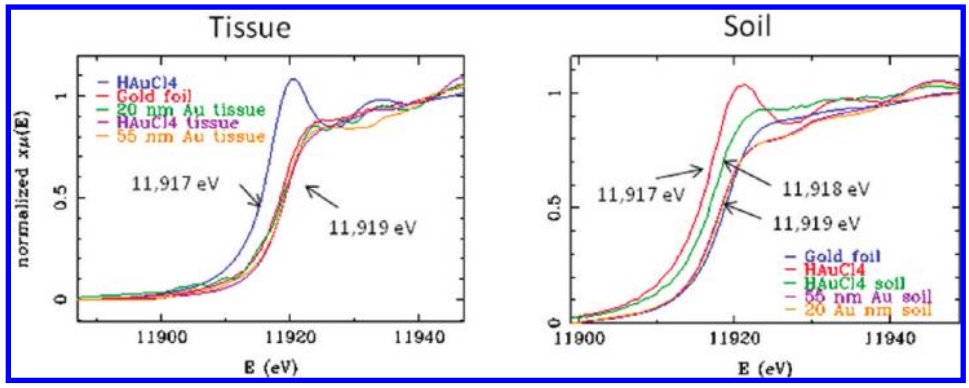

FIGURE 2. Example micro-X-ray absorption near edge spectra (μXANES; fluorescence mode) of Au foil and $HAuCl_4$ standards compared to μXANES from foci located within tissues of earthworms and samples of soil fortified with either $HAuCl_4$, 20 nm Au nanoparticles or 55 nm Au nanoparticles. Energy for absorption edges is given for each oxidation state of Au in the figures (Au (0) = 11 919, Au (I) = 11 918 and Au (III) = 11 917 eV).

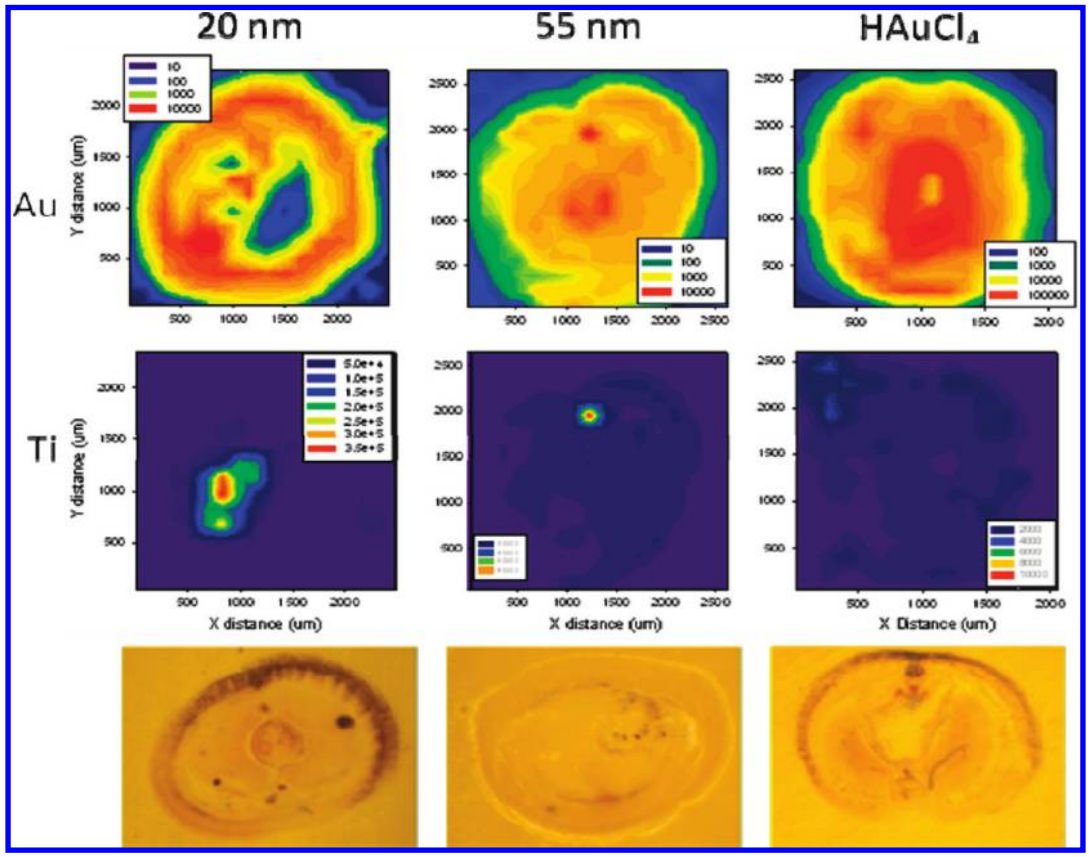

FIGURE 3. Example contour plots showing the spatial localization of Au (top row) in cross sections of earthworms exposed to either $HAuCl_4$, 20 nm Au NPs or 55 nm Au nanoparticles. The Ti intensities are also shown (middle row) to indicate the location of soil particles remaining within the gut lumen. The bottom row contains light micrographs of the sections captured using the video camera of the laser ablation system. Color bars indicate intensity of target analyte in counts per second.

only Au (0) was present within the soils fortified with Au NPs (Figure 2). The majority of spectra obtained for the $HAuCl_4$ containing soils also contained Au (0); however, some spectra were reflective of Au (I) as evidenced by the 1 eV shift in the absorption edge to 11 918 eV (Figure 2). Oxidized Au is unstable under ambient redox conditions (*13*) and it is likely that the Au (III) ions were readily reduced in the soil.

The particles were extensively aggregated in the <0.2 μm fraction of the pore water (SI Figure S3). The majority of particles in the 20 nm treated soil ranged from 60−150 nm, while the particle sizes in the 55 nm treated soil pore water ranged from 50−120 nm. The peak in the AF4 fractograms for the 20 nm soil pore water was at approximately 100 nm, while for the 55 nm treated pore water it was approximately 55 nm, which was similar to primary particle size (SI Figure S3). The 20 nm pore water also contained a greater proportion of material greater than 150 nm in diameter as indicated by the relative intensity of the release peak. We were only able to obtain a high enough signal for quantification at the highest exposure concentrations. The total Au concentrations in the pore water were 8.0 and 3.4% of the bulk soil concentrations for 20 and 55 nm Au NP treated soils, respectively. Recovery from the AF4 channel ranged from 70 to 83%.

Au Accumulation in Earthworms. Uptake of Au NPs and $HAuCl_4$ was clearly related to exposure concentration and was far greater for $HAuCl_4$ than for AuNPs (Figure 1). There was no clear primary particle size dependence for accumulation on a mass concentration basis, although on a particle number basis, many more 20 nm particles would have been taken up than 55 nm particles given an equal

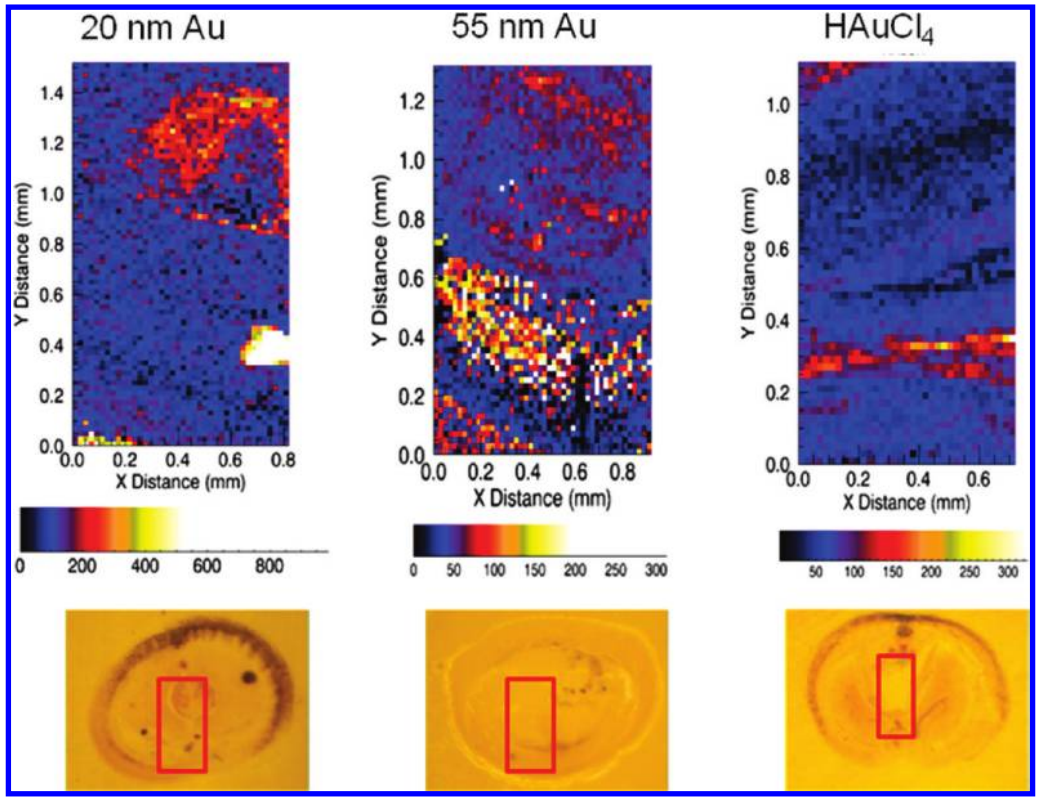

FIGURE 4. Example scanning X-ray fluorescence micrographs of showing the spatial localization of Au in cross sections of earthworms exposed to either $HAuCl_4$, 20 nm Au NPs or 55 nm Au nanoparticles. Color bars indicate the Au $L_{\alpha 1}$ fluorescence in normalized counts per second after correction for interference from Zn $K_{\beta 1}$ fluorescence. The graphs transect a 0.8 mm wide region from the body wall (bottom) to the gut (top). The region located at 0.8, 0.4 mm in the 20 nm micrograph contained high concentrations of Ti and was likely a soil particle. Regions of interest in the tissue cross sections represented in the scan are shown outlined in red in the light micrographs of the tissue sections shown below.

mass concentration (volume of a 20 nm sphere is 20.8 times that of a 55 nm sphere). The accumulated concentrations were nearly identical between particle sizes at the lowest concentration but were higher for 20 nm at the intermediate exposure and higher for 55 nm at the highest exposure concentration. This may be related to our observation at the highest exposure concentration where the 20 nm particles were more extensively aggregated in the soil pore water than the 55 nm particles and had a larger average hydrodynamic diameter (SI Figure S3). Our previous study suggested that 18 nm Au NPs were less bioaccumulative than 4 nm Au NPs in *Eisenia fetida* (*24*); however, we did not determine the aggregate size in that study. Another previous study on uptake of oxidized Cu NPs in earthworms exposed to Cu NPs also failed to show that uptake was dependent on primary particle size; however, this study did not quantitatively determine what contribution to the body burdens was due to Cu^{2+} ions versus oxidized Cu NPs (*21*). A cell culture based study suggested that there is an optimal diameter for uptake into HeLa cells via endocytosis of about 50 nm (*25*). In contrast, a study in whole mice exposed via drinking water showed that 4 nm Au NPs were absorbed to a much greater extent than 10−58 nm Au NPs, and there was a trend of decreased uptake with increasing size over the range of 10−58 nm (*26*). These studies did not investigate the aggregate size of Au NPs in the exposure media. Such characterization is particularly difficult in complex media such as soil pore waters that contain naturally occurring colloids. Continued development of improved methods to quantify aggregation state in soils and sediments at trace concentrations are needed to help identify the processes that influence NP bioavailability in soil.

Spatial Localization and Speciation of Au in Tissues. The LA-ICP-MS analyses demonstrated that Au was distributed throughout the earthworm cross section for all materials (Figure 3). The regions with the greatest intensity tended to be within the gut (Figure 3). The distribution of Ti is also shown to indicate the location of soil remaining within the gut lumen and these are the areas of the highest Au intensity; however, it is clear that Au is present outside of the gut lumen throughout the body demonstrating true uptake and biodistribution. The concentrations of Au within gut tissue of the $HAuCl_4$ treated animals were also much greater than in NP treated animals, suggesting differences in the uptake, distribution and elimination mechanisms between Au ions and NPs.

The μXANES data unequivocally demonstrated the presence of Au metal in the earthworm tissues for both treatments. The spectra for hotspots identified in the earthworm tissue were virtually identical to the spectra for Au metal (Figure 2). The $HAuCl_4$ standard had a peak above the absorption edge which is diagnostic for the presence of and Au (III) and does not occur in the spectrum of Au metal (*27*). Further, the inflection points of the absorption edges for the spectra obtained from tissues were all similar to that for Au (0) (11,919 eV) (Figure 2). We also noted that Au metal was present within the $HAuCl_4$ exposed animals; however, the spatial distribution of Au was much less punctuate than for the Au NP exposed animals and concentrations were consistently greater (Figure 3, Figure 4). It has previously been established that Au^{1+} and Au^{3+} can be taken up from soil by plants, but Au is subsequently reduced to metal within the tissue (*27, 28*). To our knowledge, this is the first evidence that this process also occurs in animals.

TEM Analysis of Tissues. For both the 20 and 55 nm Au treatments, we observed electron dense features within the gut epithelial cells that were similar in diameter to the respective particles to which the animals were exposed (SI

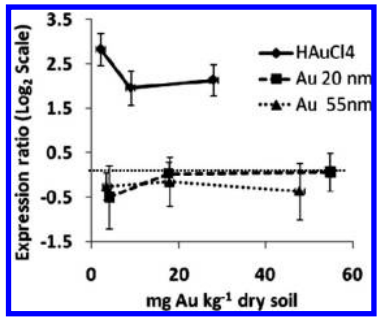

FIGURE 5. Metallothionein expression ratios for earthworms exposed to $HAuCl_4$, 20 nm Au nanoparticles or 55 nm Au nanoparticles as a function of Au concentration in soil. Error bars indicate standard errors. All ratios for $HAuCl_4$ exposed animals are significantly higher than in controls ($p < 0.05$), while expression ratios are not significantly different from controls for 20 and 55 nm Au nanoparticle exposed animals. The dotted horizontal line indicates an expression ratio of zero.

Figures S4 and S5). These tended to occur as isolated particles or as aggregates of 2−7 particles within the cytoplasm. The EDS spectra for selected electron dense features, confirmed their identity as Au. Electron dense features similar to those observed for the Au NP treated tissues were not typically observed in the control tissues (SI Figure S6).

Biological Responses. The qRT-PCR analyses validate the lack of a role of Au ions in exposure, or subsequent subcellular dissolution for Au NP exposed animals. While we observed clear upregulation of mtl as a result of $HAuCl_4$ exposure, there was no upregulation of mtl from Au NP exposure (Figure 5). Metallothionein is a cysteine rich protein which is upregulated in response to metal ion exposure in earthworms and plays a role in metal homeostasis and detoxification (*29*). Although Au (I) or Au (III) were not detected in tissue from the $HAuCl_4$ treatment, it is possible that they were taken up and subsequently reduced to Au metal, or that the oxidized forms occurred in concentrations that were too low to obtain usable μXANES spectra. The data presented here help to confirm the spectroscopic evidence from μXANES analysis that the Au detected in tissues from the Au NP treatments was taken up NP form, rather than ionic form. It also demonstrates that the Au metal detected in tissues from the $HAuCl_4$ treatment were taken up by the earthworms at least in part as Au ions. We did not observe statistically significant ($p < 0.05$) changes for any of the other genes related to oxidative or cellular stress. Previous studies in earthworms exposed to metals have demonstrated transient upregulation of genes that subsides over the course of prolonged exposure, so time-resolved studies should be undertaken in the future (*30*).

We observed no statistically significant effects of any of the treatments on earthworm body mass. There was sporadic mortality in some of the treatments (20% for 5 mg kg^{-1}, 20 nm Au and 14% for 62 mg kg^{-1} 55 nm Au) that was neither concentration dependent nor statistically significant (control mortality was 3.4%); therefore, we concluded that this mortality was not likely the result of exposure. We observed concentration dependent changes in reproduction in the $HAuCl_4$ treatment where reproduction was significantly greater ($p < 0.05$) than in controls at the lowest exposure concentration and significantly lower than in controls at the highest exposure concentration (Figure 6). These changes did not directly correlate with the sporadic mortality. Statistically significant decreases in reproduction were also observed at the highest exposure concentration for 20 nm Au NPs and for the intermediate exposure concentration for 55 nm Au NPs. While further studies are needed to assess concentration−response relationships it appears that both $HAuCl_4$ and Au NPs are capable of affecting reproduction in

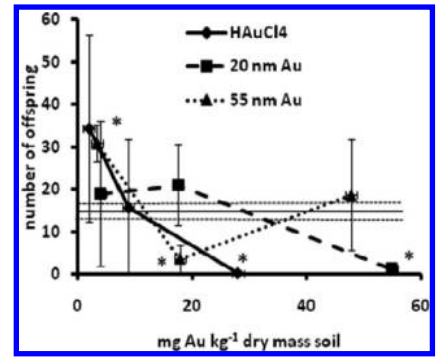

FIGURE 6. Number of offspring produced at 56 days for earthworms exposed to $HAuCl_4$, 20 nm Au NPs or 55 nm Au NPs as a function of Au concentration in soil. Error bars indicate standard deviations. Asterisks indicate data that are significantly different from controls ($p < 0.05$). Solid horizontal line indicates mean number of offspring for controls and dashed horizontal lines indicate one standard deviation from the control mean.

E. fetida. The present study only assessed total production of juveniles after 56 days of exposure; therefore, effects could be manifested through suppression of cocoon production, hatchability, or juvenile survival. Adverse effects of nanomaterials (multiwalled carbon nanotubes) on reproduction in earthworms have previously been demonstrated, where there was also a lack of monotonic concentration dependence (*31*).

The evidence presented here clearly demonstrates the bioavailability of Au NPs in soil and highlights the utility of using Au NPs as tracers to examine the environmental behavior of nanoparticles. Earthworms are important ecological receptor species that play a key role in the structure and function of terrestrial ecosystems. Evidence that intact nanomaterials can be absorbed by earthworms and biodistributed to tissues remote from the portal of entry highlights the importance of considering food chain accumulation and trophic transfer when assessing the ecological risks of nanomaterials. While previous studies have suggested the entry of nanomaterials into food webs (*15, 21, 32*), this is one of the first studies to demonstrate the true uptake and biodistribution of nanomaterials by detritivores in an environmentally realistic exposure scenario with potential effects on an ecologically relevant end point. Future development of methods for characterizing the physicochemical properties of nanomaterials in soil and sediment pore water will help to provide insight into factors governing bioavailability.

Acknowledgments

We acknowledge the advice and assistance of A. Lanzirotti, J. Judy, D. Addis, M. Engle, D. Karapatakis, and three anonymous reviewers. Major funding was provided by the U.S. Environmental Protection Agency—Science to Achieve Results Grant No. RD833335. Support was also provided by the National Science Foundation and U.S. EPA through the Center for Environmental Implications of Nanotechnology (CEINT; EF-0830093). Portions of this work were performed at Beamline X26A, National Synchrotron Light Source (NSLS), Brookhaven National Laboratory. X26A is supported by the U.S. Department of Energy (DOE)-Geosciences (DE-FG02-92ER14244 to The University of Chicago-CARS) and DOE-Office of Biological and Environmental Research, Environmental Remediation Sciences Division (DE-FC09-96-SR18546 to the University of Kentucky). The use of the NSLS was supported by DOE under contract no. DE-AC02-98CH10886.

Supporting Information Available

Supplemental experimental methods (nanoparticle characterization, bulk ICP-MS analyses, asymmetrical flow field

flow fractionation analysis, bioassay methods, X-ray microanalysis); TEM images of study materials (Figure S1); XANES of stock suspensions (Figure S2); TEM and EDS for gut tissues from 20 nm treatment (Figure S3), the 55 nm treatment (Figure S4), and TEM from the control treatment (Figure S5). This material is available free of charge via the Internet at http://pubs.acs.org.

Literature Cited

(1) *Nanotechnology White Paper*, EPA 100/B-07/001; U.S. Environmental Protection Agency: Washington, DC, 2007.

(2) Wiesner, M. R.; Lowry, G. V.; Alvarez, P.; Dionysiou, D.; Biswas, P. Assessing the risks of manufactured nanomaterials. *Environ. Sci. Technol.* **2006**, *40* (14), 4336–4345.

(3) Colvin, V. The potential environmental impact of engineered nanomaterials. *Nat. Biotechnol.* **2003**, *21* (10), 1166–1170.

(4) *Environmental, Health, and Safety Research Needs for Engineered Nanoscale Materials*; National Science and Technology Council: Washington, DC, 2006.

(5) Benn, T. M.; Westerhoff, P. Nanoparticle silver released into water from commercially available sock fabrics. *Environ. Sci. Technol.* **2008**, *42* (11), 4133–4139.

(6) Kiser, M. A.; Westerhoff, P.; Benn, T.; Wang, Y.; Perrez-Rivera, J.; Hristovski, K. Titanium nanomaterial removal and release from wastewater treatment plants. *Environ. Sci. Technol.* **2009**, (43), 6757–6783.

(7) Mueller, N.; Nowack, B. Exposure modeling of engineered nanoparticles in the environment. *Environ. Sci. Technol.* **2008**, *42* (12), 4447–4453.

(8) *A Guide to the Biosolids Risk Assessments for the EPA Part 503 Rule*; U.S. Environmental Protection Agency.: Washington, DC, 1995.

(9) Gottschalk, F.; Sonderer, T.; Scholz, R. W.; Nowack, B. Modeled environmental concentrations of engineered nanomaterials (TiO_2, ZnO, Ag, CNT, Fullerenes) for different regions. *Environ. Sci. Technol.* **2009**, *43* (24), 9216–9222.

(10) Murphy, C. J.; San, T. K.; Gole, A. M.; Orendorff, C. J.; Gao, J. X.; Gou, L.; Hunyadi, S. E.; Li, T. Anisotropic metal nanoparticles: Synthesis, assembly, and optical applications. *J. Phys. Chem. B.* **2005**, *109* (29), 13857–13870.

(11) Everts, M.; Saini, V.; Leddon, J. L.; Kok, R. J.; Stoff-Khalili, M.; Preuss, M. A.; Millican, C. L.; Perkins, G.; Brown, J. M.; Bagaria, H.; Nikles, D. E.; Johnson, D. T.; Zharov, V. P.; Curiel, D. T. Covalently linked Au nanoparticles to a viral vector: Potential for combined photothermal and gene cancer therapy. *Nano Lett.* **2006**, *6* (4), 587–591.

(12) Gao, D.; Agayan, R. R.; Xu, H.; Philbert, M. A.; Kopelman, R. Nanoparticles for two-photon photodynamic therapy in living cells. *Nano Lett.* **2006**, *6* (11), 2383–2386.

(13) Krauskopf, K. The solubility of gold. *Econ. Geol.* **1951**, *46* (8), 858–870.

(14) Connor, E. E.; Mwamuka, J.; Gole, A.; Murphy, C. J.; Wyatt, M. D. Gold nanoparticles are taken up by human cells but do not cause acute cytotoxicity. *Small* **2005**, *1* (3), 325–327.

(15) Ferry, J. L.; Craig, P.; Hexel, C.; Sisco, P.; Frey, R.; Pennington, P. L.; Fulton, M. H.; Scott, I. G.; Decho, A. W.; Kashiwada, S.; Murphy, C. J.; Shaw, T. J. Transfer of gold nanoparticles from the water column to the estuarine food web. *Nat. Nanotech.* **2009**, *4* (7), 441–444.

(16) Sau, T.; Murphy, C. Seeded high yield synthesis of short Au nanorods in aqeuous solution. *Langmuir* **2004**, *20*, 6414–6420.

(17) Jana, N. R.; Gearheart, L.; Murphy, C. J. Seeding growth for size control of 5−40 nm diameter gold nanoparticles. *Langmuir* **2001**, *17* (22), 6782–6786.

(18) *Guideline for the Testing of Chemicals: Earthworm Reproduction Test (Eisenia fetida)*; Organization for Economic Cooperation and Development: Paris, 2004.

(19) *Method 3052: Microwave Assisted Acid Digestion of Siliceous and Organically Based Matrices*; U.S. Environmental Protection AgencyWashington, DC, 1996.

(20) *Method 6020a: Inductively coupled plasma - mass spectrometry*; U.S. Environmental Protection Agency: Washington, DC, 1998.

(21) Unrine, J.; Tsyusko, O.; Hunyadi, S.; Judy, J.; Bertsch, P. M. Effects of particle size on chemical speciation and bioavailability of Cu to earthworms (*Eisenia fetida*) exposed to Cu nanoparticles. *J. Environ. Qual.* **2010**, doi: 10.2134/jeq2009.0387.

(22) Ravel, B.; Newville, M. Athena, Artemis, Hephaestus: data analysis for X-ray absorption spectroscopy using IFEFFIT. *J. Synchrotron Radiat.* **2005**, *12*, 537–541.

(23) Pfaffl, M. W.; Horgan, G. W.; Dempfle, L. Relative expression software tool (REST(C)) for group-wise comparison and statistical analysis of relative expression results in real-time PCR. *Nucl. Acids. Res.* **2002**, *30* (9), e36.

(24) Unrine, J.; Bertsch, P.; Hunyadi, S. Bioavailability, trophic transfer, and toxicity of manufactured metal and metal oxide nanoparticles in terrestrial environments. In *Nanoscience and Nanotechnology: Environmental and Health Impacts*; Grassian, V., Ed.; John Wiley and Sons, Inc: Hoboken, 2008.

(25) Chithrani, B. D.; Ghazani, A. A.; Chan, W. C. W. Determining the size and shape dependence of gold nanoparticle uptake into mammalian cells. *Nano Lett.* **2006**, *6* (4), 662–668.

(26) Hillyer, J. F.; Albrecht, R. M. Gastrointestinal persorption and tissue distribution of differently sized colloidal gold nanoparticles. *J. Pharm. Sci.* **2001**, *90* (12), 1927–1936.

(27) Gardea-Torresdey, J. L.; Rodrigues, E.; Parsons, J. G.; Peralta-Videa, J. R.; Meitzner, G.; Cruz-Jimenez, G. Use of ICP and XAS to determine the enhancement of gold phytoextraction by *Chilopsis linearis* using thiocyanate as a complexing agent. *Anal. Bioanal. Chem.* **2005**, *382*, 347–352.

(28) Gardea-Torresdey, J. L.; Parsons, J. G.; Gomez, E.; Peralta-Videa, J.; Troiani, H. E.; Santiago, P.; Yacaman, M. J. Formation and growth of Au nanoparticles inside live alfalfa plants. *Nano Lett.* **2002**, *2* (4), 397–401.

(29) Dallinger, R.; Berger, B.; Gruber, C.; Hunziker, P.; Sturzenbaum, S. Metallothioneins in terrestrial invertebrates: Structural aspects, biological significance and implications for their use as biomarkers. *Cell. Mol. Biol.* **2000**, *46* (2), 331–346.

(30) Brulle, F.; Mitta, G.; Cocquerelle, C.; Vieau, D.; Lemiere, S.; Lepretre, A.; Vandenbulcke, F. Cloning and real-time PCR testing of 14 potential biomarkers in *Eisenia fetida* following cadmium exposure. *Environ. Sci. Technol.* **2006**, *40* (8), 2844–50.

(31) Scott-Fordsmand, J. J.; Krogh, P. H.; Schaefer, M.; Johansen, A. The toxicity testing of double-walled nanotubes-contaminated food to *Eisenia veneta* earthworms. *Ecotoxicol. Environ. Saf.* **2008**, *71* (3), 616–619.

(32) Holbrook, R. D.; Murphy, K. E.; Morrow, J. B.; Cole, K. D. Trophic transfer of nanoparticles in a simplified invertebrate food web. *Nat. Nanotechnol.* **2008**, *3* (6), 352–355.

ES101885W